Molecular Dynamics Study of Free Energy Profiles for Organic Cations in Gramicidin A Channels

Yili Hao, Michael R. Pear, and David D. Busath
Brown University, Department of Physiology, Providence, Rhode Island 02912

ABSTRACT The free energy profiles for four organic cations in right-handed single-helix gramicidin A dimers were computed by using umbrella sampling molecular dynamics with CHARMM. Ion-water column translocations were facilitated by using a novel "water-tunnel" approach. The overlapping pieces of free energy profile for adjacent windows were selected from three trajectories that differed in initial ion rotation and were aligned by the method of umbrella potential differences. Neglected long-range electrostatic energies from the bulk water and the bilayer were computed with DelPhi and added to the profile. The approach was corroborated for the formamidinium-guanidinium pair by using perturbation dynamics at axial positions 0, 6, 12, and 15 Å from the channel center. The barrier to ethylammonium entry was prohibitive at 21 kcal/mol, whereas for methylammonium it was 5.5 kcal/mol, and the profile was quite flat through the channel, roughly consistent with conductance measurements. The profile for formamidinium was very similar to that of methylammonium. Guanidinium had a high entry barrier ($\Delta F = +8.6$ kcal/mol) and a narrow deep central well ($\Delta F = -2.6$ kcal/mol), qualitatively consistent with predictions from voltage-dependent potassium current block measurements. Its deep central well, contrasting with the flat profile for formamidinium, was verified with perturbation dynamics and was correlated with its high propensity to form hydrogen bonds with the channel at the dimer junction (not shared by the other three cations). Analysis of the ensemble average radial forces on the ions demonstrates that all four ions undergo compressive forces in the channel that are at maximum at the center of the monomer and relieved at the dimer junction, illustrating increased flexibility of the channel walls in the center of the channel.

INTRODUCTION

The free energy profile, equivalent to the potential of mean force (PMF), has become a central concept in understanding the ion transport through channels (Eyring et al., 1949; Hille, 1992; for a brief review of the gramicidin applications, see Busath, 1993), providing a direct link with the statistical mechanics theory of dynamical rate process in liquids. The fact that the gramicidin channel consists of a small peptide of known structure makes it possible to compute the PMF profile for ion permeation by using an empirical force field with an atomistic model. Zero-degree (adiabatic mapping) potential energy profiles (e.g. Kim et al., 1985; Etchebest et al., 1984; Etchebest and Pullman, 1988; Turano et al., 1992) are an approximation to the free energy profile. Molecular dynamics studies more accurately yield the PMF for alkali metal cation transport by implicitly including entropy and the dynamic average potential energy (Åqvist and Warshel, 1989; Roux, 1990; Jordan, 1990; Roux and Karplus, 1991a,b, 1993; Dorman et al., 1996). Early calculations resulted in excessive energy barriers (see Jordan, 1987, 1990), possibly because of force-field imbalances between the large ion-water and ion-peptide interaction energies. Åqvist and Warshel (1989) computed the free energy of solvating Na^+ by gramicidin A (simulated as a left-handed helical dimer of polyglycine) and found that the activation barrier for Na^+ entry is less than 5 kcal/mol, in agreement with the barriers derived from experimentally observed permeation rates (Bamberg and Läuger, 1974; Eisenman and Sandblom, 1983; Eisenman and Horn, 1983). Roux and Karplus (1993) found a series of 5 kcal/mol barriers for transport of Na^+ through the channel and negligible barriers for transport of K^+, consistent with experiment, but found a ~12 kcal/mol barrier to Na^+ entry (essentially a square translocation barrier); this is larger than would be consistent with observed permeation rates (Roux and Karplus, 1994). Dorman et al. (1996) implemented a semimicroscopic approach to calculating the PMF in which they carried out free energy calculations incorporating an exact treatment of the long-range electrostatic contributions due to interactions with both low dielectric lipid and high dielectric aqueous domains, and combined these with experimental hydration energy data. This approach yielded reasonable (albeit coarse) free energy profiles for K^+, Rb^+, and Cs^+ and for several anions in the channel. Not only did cation profiles correlate with experimental evidence, but they identified the source of valence selectivity in the gramicidin channel.

Small organic cations have served as useful probes in the study of ion-gramicidin channel interactions in previous research (Myers and Haydon, 1972; Eisenman et al., 1976;

Received for publication 29 July 1996 and in final form 8 July 1997.

Address reprint requests to Dr. David Busath, Zoology Department, Brigham Young University, Provo, UT 84602. Tel.: 801-378-8753; Fax: 801-378-7423; E-mail: david_busath@byu.edu.

Dr. Hao's present address is Laboratory of Mathematical Biology, National Cancer Institute, Bldg. 12B, Rm. B116, 12 South Drive, National Institutes of Health, Bethesda, MD 20892-5677.

Dr. Pear's present address is Molecular Simulations, 9685 Scranton Rd., San Diego, CA 92122.

Dr. Busath's present address is Zoology Department, Brigham Young University, Provo, UT 84602.

0006-3495/97/10/1699/18 $2.00

Busath et al., 1988; Hemsley and Busath, 1991; Turano et al., 1992; Seoh and Busath, 1993a,b, 1995). In the present study, we use four small monovalent organic cations (Fig. 1), methylammonium, ethylammonium, guanidinium, and formamidinium, to explore the steric selectivity mechanism of the gramicidin A channel. They have dimensions (Fig. 1) comparable to the internal diameter of the gramicidin channel pore. The channel diameter has been estimated variously from plastic van der Waals models as ~4 Å (Urry, 1984), from a vacuum energy-minimized structure using hard core atomic radii as 3.7 Å minimum (Busath et al., 1988; Turano et al., 1992), and from the channel structure in sodium dodecyl sulfate (SDS) micelles (Arseniev et al., 1986) refined with a Monte Carlo simulated annealing procedure and using hard core radii as 2.82 Å minimum (Smart et al., 1993). In the last paper, the method revealed that for the Arseniev conformation the channel lumen is narrowest at a point ~11 Å from the center of the channel and widens uniformly to a hard core radius of 4.32 Å at the center of the channel. A similar trend was noticed in the model structure developed by Turano et al. (unpublished results). Whether the spindle-shaped pore suggested by the modeling and SDS micelle structure occurs in bilayers is open to debate. In fact, a structure recently determined by solid-state NMR (Ketchum et al., 1996) has a uniform cylindrical hard core pore of diameter 4.0–4.2 Å. However, the computations presented here were performed on the spindle-shaped SDS micelle structure, and no attempt has yet been made to compare results between models.

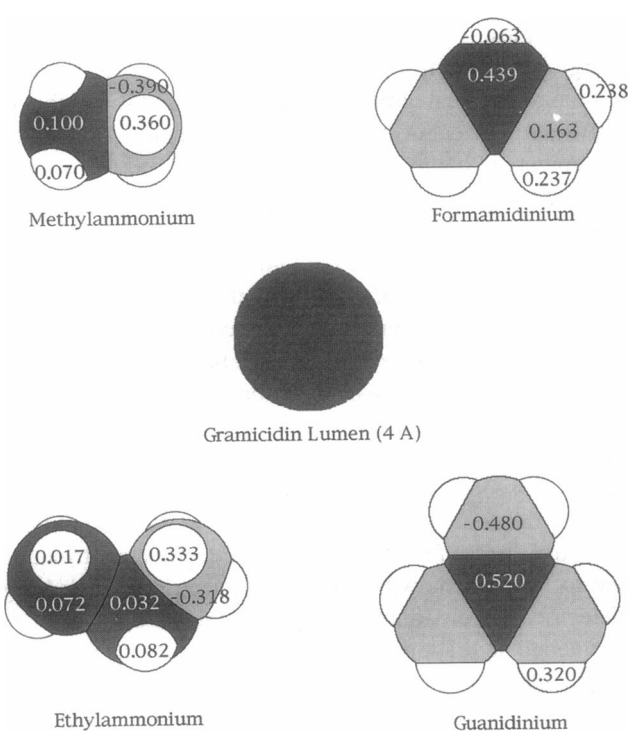

FIGURE 1 Space-filling structures (using van der Waals radii) of the four organic cations used in this study. Partial charges are labeled. The approximate van der Waals lumen of the gramicidin A channel (4 Å) is provided for reference. It should be noted that the van der Waals radius reflects the optimal contact distance rather than the hard shell atomic radius.

The four cations have different sizes and shapes, resulting in different electrophysiological behavior when they pass through gramicidin channels. In particular, the steric fit for guanidinium and formamidinium ions in the channel is governed by their rigid planar character. The minimum profile hard core diameters for formamidinium and guanidinium are 4.5 Å and 5.4 Å, respectively (Hemsley and Busath, 1991) when the hydrogen bonding potential of the amide hydrogens is used to reduce the effective hydrogen radius by 0.5 Å. Thus one would expect both ions to be too large to fit through the channel, but both are planar molecules and, as shown by Turano et al. (1992), it is quite feasible for formamidinium to twist through atomic crevices to pass through the channel. Methylammonium has a minimum hard core profile diameter of 3.9 Å, and that of ethylammonium is 4.2 Å. However, methylammonium has flexibility about its dihedral angle, and its two heavy atoms can align on the channel axis, whereas ethylammonium has poor flexibility about the C-C-N angle and so is much less able to adjust to crevices than even guanidinium. The conductance properties of the four cations have been well explored (Hemsley and Busath, 1991; Seoh and Busath, 1993a,b, 1995; Busath, unpublished results for ethylammonium).

Methylammonium and formamidinium readily permeate the gramicidin channel with conductances of ~0.73 pS and 1.58 pS, respectively, at 10 mM and 100 mV (Seoh and Busath, 1993a). These are comparable to the conductances of Na^+ (0.83 pS) and K^+ (2.18 pS) ions under the same conditions. Ethylammonium shows no detectable conductance through the gramicidin channel (Busath et al., unpublished data). Guanidinium is scantily permeant, but it causes voltage-relieved flicker blocks of potassium-mediated currents (Hemsley and Busath, 1991). From the average block rate and duration, guanidinium passage was estimated to be $\sim 10^6$ times less frequent and longer lasting than formamidinium passage at a given voltage. There is no block effect in the case of ethylammonium, suggesting that ethylammonium is not even able to enter the gramicidin channel, nor does it dwell for long times (ms) at the mouth of the channel. Formamidinium was found to induce gramicidin A channel stabilization (i.e., the channel lifetimes in the presence of formamidinium are much longer than with K^+, ammonium, methylammonium, etc.) and significant single-channel noise (Seoh and Busath, 1993b). The noise is presumably due to fluctuations in channel structure induced by formamidinium and involves the tryptophan side chains near the entries, judging by the absence of these effects in gramicidin M^- channels, in which the tryptophans are replaced by phenylalanines.

Potential energy computations using the adiabatic mapping approach suggest that there is a barrier to guanidinium and formamidinium entry associated with the first (C-terminal) turn of the channel β-helix (Turano et al., 1992). The guanidinium potential energy barrier is ascribed to the dis-

ruption of the intramolecular hydrogen bonding near the C-terminus of the peptide as the cations enter the channel. The ions are expected to tilt and twist to pass through the channel.

In a preliminary study, Pear and Busath (1990) used the umbrella sampling method to compute the PMF for guanidinium and formamidinium and found a 9 kcal/mol entry barrier for guanidinium and 4 kcal/mol for formamidinium located just inside the channel entry. The activation free energy barriers reported in this work have similar heights; however, the shape of the free energy profiles differ in that the barrier for guanidinium in particular is much broader. The window-overlap matching method used in that preliminary study to link pieces of the free energy profile together is expected to be less accurate than the umbrella potential differences method employed here. In addition, the translocation protocol differed in that the starting structure of each window trajectory was taken from the end of the previous window trajectory. This protocol rendered the channel vulnerable to deterioration, resulting in premature termination of the entry barrier, evidenced when compared to the findings reported here.

Gramicidin has been found to produce double-helical channels under certain unusual conditions (Saberwal et al., 1995; Durkin et al., 1992), but most conductance studies, including those with organic cations, utilize the single-helix head-to-head dimer form. Although certain variants of gramicidin A are known to form left-handed helices (Saberwal et al., 1995; Koeppe et al., 1992), most, including gramicidin A, form right-handed helices (Arseniev et al, 1986; Tucker et al., 1992; Urry, 1992). The right-handed head-to-head dimer of single helices was used for free energy computations in this study.

The free energy profiles for each of four organic cations were calculated by using umbrella sampling molecular dynamics utilizing a system consisting of the gramicidin dimer, with capping water balls at each end containing vacant pores coaxial with the channel. This system is transected by a molecular column consisting of the ion and a row of waters passing through the channel and the pores in the capping water balls. This method of managing the waters is a novel contribution of this work and allows a consistent degree of equilibration and efficient translation of the ion through the channel. The perturbation method allows cross-checking of the free energy difference between formamidinium and guanidinium, obtained by umbrella sampling at several points inside and just outside of the channel. Free energy decomposition and force analysis are utilized to understand the source of the barriers. A common problem in the molecular dynamics simulations, due to limited computer power, is that few if any solvent molecules are usually included. Although the Coulomb interaction energy decreases as the first power of distance, the number of polarized water molecules increases as the second power of distance; hence the neglected long-range electrostatic energies can play an important role in the free energy profile. Here we use DelPhi (Klapper et al., 1986; Gilson and Honig, 1988; Gilson et al., 1988), a finite-differences solution to the nonlinear Poisson-Boltzmann equation, to estimate the neglected long-range electrostatic interaction energies of the bulk water and lipid membrane.

Traditional approaches such as the Nernst-Planck continuum diffusion equation (Levitt, 1982, 1991) or Eyring rate theory (Läuger, 1973; Urban and Hladky, 1979; Becker et al., 1992) provide useful phenomenological tools to account for the electrophysiological properties of the channel; however, the phenomenological approach fails to yield a microscopic picture of the mechanisms involved in ion transport. Effective analysis of channel characteristics requires the identification of the system components and the specific kinds of interactions that regulate ion flow. Molecular dynamics simulation studies based on detailed atomic models provide an opportunity to explore the detailed atomic interactions responsible for channel selectivity. A decomposition of the ion-channel interaction is explored here to reveal the mesoscopic picture of the mechanism behind the free energy profiles, particularly that of steric hindrance, which plays an important role in "tight-fit" selectivity. Steric hindrance can be conceptualized in terms of radial compressive forces from the environment on the permeating solute. Preliminary reports of these results were published previously (Hao and Busath, 1996; Hao, 1996).

MODEL DESCRIPTION AND COMPUTATIONAL DETAIL

Gramicidin model

The positions of the gramicidin A channel atoms were computed according to the docking parameters and backbone dihedral angles for the right-handed $\beta^{6.3}$ helix dimer deduced from ^{1}H NMR (Arseniev et al., 1986). There are 316 atoms in the dimer. Hydrogen atoms are explicitly included only if they are polar, and the effects of nonpolar hydrogen atoms are included implicitly by use of extended carbons. Side chains and terminators were included. The channel was initially oriented to be centered on the origin, with the long axis oriented along the x axis. Bond and atom parameters were from Quanta 3.2 (Molecular Simulations, Burlington, MA) (Momany and Rone, 1992).

Organic cation models and water

The organic cation structures and partial charges are summarized in Fig. 1. Methylammonium and ethylammonium structures were built from standard parameters using Quanta 3.2, with the partial charges computed using the rules-based algorithm (Momany and Rone, 1992). Guanidinium and formamidinium structures were derived from the guanidino of the standard CHARMM arginine. Standard CHARMM parameters were assigned to these four ions for the bond lengths, bond angles, dihedral and improper dihedral angles, and the associated force constants. For guanidinium and formamidinium, improper dihedrals are used to control out-

of-plane bending and maintain the planarity. The ions were initially placed near the origin, i.e., near the center of the channel.

The solvent water molecules were selected from a pre-equilibrated droplet structure from MSI. All are CHARMM TIP3-type waters (Jorgensen et al., 1983), with a partial charge on oxygen of −0.834 and a partial charge on hydrogen of 0.417, resulting in a neutral molecule. There are, altogether, 217 water molecules, with 187 of them forming two water balls (~13 Å in diameter) apposed to the two channel entrances. The other 30 water molecules form a row with oxygens on the channel axis, hydrogens randomly oriented, separated by ~3.3 Å, extending well beyond the two water balls. At the center of the row, which was initially located at the origin, the separation between waters was suitably enlarged to accommodate the ion. The dipoles of the two waters immediately adjacent to the ion, unmodified TIP3 waters, were aligned with the negative end near the cation charge.

Recent theoretical analysis of water orientations in a gramicidin channel containing a single ion indicates that all channel waters would probably be polarized by the ion (Dorman et al., 1996); however, our equilibration runs were not long enough to allow derandomization of the two to five nonoriented channel waters. This factor may affect the overall free energy profile; however, it should have little impact on the conclusions regarding steric hindrance, which depend primarily on local ion-channel interactions.

The entire system

Fig. 2 shows the structure of the whole system. The gramicidin dimer extends to ±12.5 Å along the x axis, with the two water balls situated at the channel mouths extending to ± 25 Å; these partially model the solvent environment. The whole system is transected by the axial water column, which extends to ± 48 Å. About eight of these water molecules are inside the channel, four on each side of the ion. The ion-water column was translated as a unit in the initial channel/water balls structure to a new position to initiate each new umbrella sampling window. This procedure prevented progressive equilibration of the ion-water-channel conformation during ion translocation, while providing a clearly defined conformation and prevented artificial deterioration of peptide structures such as inter-

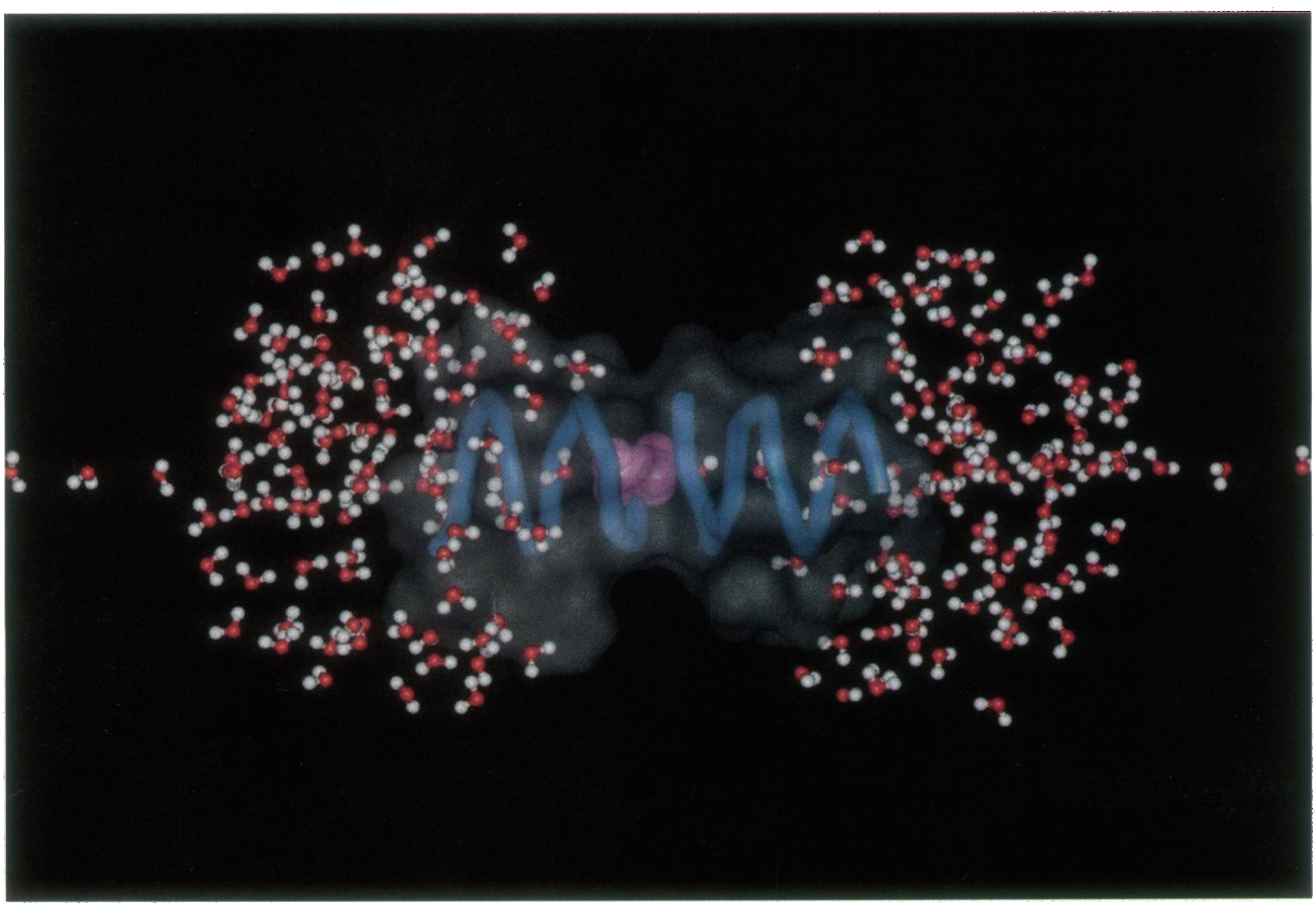

FIGURE 2 View of the molecular system used for all CHARMM calculations, including the gramicidin dimer, column, and bulk water, and a representative cation. The water column is extended beyond the bulk water hemispheres for convenience in translation. Created with Molecular Simulations WebLab Viewer, v. 2.0.

monomer hydrogen bonds. For the simulation at each window, the water column extends to at least the edge of the channel-solvent system. After translation, column water molecules that were still outside the water balls were cut out in the computations for methylammonium and ethylammonium (and for the neutral methylamine), but not for guanidinium and formamidinium, because this procedure turned out to have a negligible effect on the PMF.

Although no constraints were applied (except for the window potential) during the dynamic simulations, the system remained essentially intact, with no more than one or two water molecules dissociating from the system and minimal changes in peptide hydrogen bonding or side-chain conformation during the 10-ps simulation.

Quanta 3.2 and 3.3 were used to construct the system model. CHARMM (Department of Chemistry, Harvard University, versions 22 and 23) was modified to include the umbrella potential term,

$$U(x) = k(x - x_0)^2 \tag{1}$$

where x is the axial distance of a reference atom in the cation from the midpoint of the two centers of gramicidin monomer mass and x_0 is the desired or "window" position, and a supplemental harmonic potential for deviations of the "channel axis," defined as the line connecting the two centers of gramicidin monomer mass, from the x axis to hold the channel to the x axis for convenience in calculating ion positions. The force constant k was set to 20 kcal/mol Å^2 for the umbrella potential holding the ion and 500 kcal/mol Å^2 for the supplemental potential. The reference atoms were the carbon in the case of methylammonium, formamidinium, or guanidinium and the nitrogen in the case of ethylammonium.

All molecular dynamics computations were carried out with the Verlet algorithm with a 1-fs time step. The nonbonded pair list was limited to 15-Å separations, which were updated every 20 fs, and nonbonded interaction energies were modulated smoothly to zero between 11 Å and 14 Å with the CHARMM "switch" functions. Water O-H bond lengths were regulated with the SHAKE algorithm (Brooks et al., 1983).

Computations

Umbrella sampling

The umbrella sampling technique (Patey and Valeau, 1975; Northrup et al., 1982; Crouzy et al., 1994) was used to compute the ion-transport potential of mean force, $W(\zeta)$, where ζ is the unidimensional reaction coordinate, which in our case is simply defined as the x coordinate of the ion reference atom. The unbiased PMF from the ith window is

$$W_i(\zeta) = -k_B T \ln[\langle \rho * (\zeta)\rangle_i] - U_i(\zeta) + \text{Ç}_i \tag{2}$$

where the constant Ç$_i$ is equal to $-k_B T \ln [\langle e^{-\beta U_i(\zeta)}\rangle]$. The first term in Eq. 2 was derived from the biased probability density, p * (*), for the ith dynamic simulation, and the window potential was subtracted to yield $W_i(\zeta)$ to within a constant for each window. One window typically covered only a very small portion of the whole reaction path, i.e., 0.5–0.8 Å along the ion translocation pathway. Except for Ç$_1$, the constants Ç$_i$ were determined by using the adjacent window differences, [Ç$_i$ − Ç$_j$], which were computed from the dynamics simulation trajectory (Crouzy et al., 1994),

$$[\text{Ç}_i - \text{Ç}_j] = -k_B T \ln[\langle \exp(-\beta[U_i(\zeta) - U_j(\zeta)])\rangle_{(j)}] \cdot (= k_B T \ln[\langle \exp(\beta[U_i(\zeta) - U_j(\zeta)])\rangle_{(i)}]) \tag{3}$$

We noticed that in our calculations this series of [Ç$_i$ − Ç$_{i-1}$] generally determines the overall shape of the PMF profile. As noted by Crouzy et al. (1994), to evaluate [Ç$_i$ − Ç$_j$] only one ensemble (jth or ith) is needed. The other could be used to cross-check the results, although we have not done so with our data. Overlapping regions of adjacent windows, $W_i(\zeta)$, were smoothed using the weighted average as suggested by Crouzy et al. (1994), i.e.,

$$W(\zeta) = \sum_i W_i(\zeta) \frac{\langle \rho(\zeta)\rangle_{(i)}}{\sum_j \langle \rho(\zeta)\rangle_{(j)}} \tag{4}$$

In preliminary runs, we passed the ion completely through the channel (from −15 Å to +15 Å). This procedure yielded symmetrical results as expected, so for efficiency we reduced the range to 0–15 Å for the results reported here. The accuracy of the result depends critically on the degree of overlap between adjacent umbrella ensembles, so we computed ensembles with window separations of 0.2–0.1 Å, resulting in ~90 windows for the construction of each half-profile.

For each window, the ion-water column was translated to position the ion reference atom at the window, and the system was minimized with 500 steps of adopted basis Newton–Raphson minimization (Brooks et al., 1983) with a window force constant of k = 500 kcal/mol · Å^2, followed by 3 ps of Verlet heating, 8 ps of thermal equilibration, and 10 ps of unconstrained simulation (window force constant k = 20 kcal/mol · Å^2). From the latter, an ensemble of 500 configurations was generated. This usually produced a piece of PMF covering 0.5–0.8 Å (depending on the site) of the reaction coordinate. Care was taken to ensure that the sampling of the window was limited by the window potential and not the shortness of the time scale, i.e., that the expected diffusion distance for the 10-ps unconstrained simulation run ($x = (2Dt)^{1/2}$~2 Å if D is near the usual value for diffusion of small molecules in bulk, ~0.2 Å^2/ps) is greater than the length of the reaction coordinate covered. Preliminary test runs using 50-ps trajectories produced essentially equivalent results.

To compensate for the fact that 10 ps of simulation does not thoroughly explore the cation conformational space (very little rotation of the cation about the channel axis took place on this time scale), we tried up to three different ion starting orientations for each window. The flattest piece of PMF (which generally also corresponded to the lowest

($\zeta_i - \zeta_j$)) for each selected window was used to construct the whole free-energy profile on two premises: the ion would be most likely to rotate in the channel so as to take the path of least resistance; and, in a typical sampling range of ~0.6 Å for one window, a large free-energy change (>2 kcal/mol) was usually a statistical artifact of insufficient sampling. The first premise is tentative; it depends on the energy barrier to rotation, which we have not explored.

As an example of the computer time involved, each umbrella sampling half-profile, consisting of 80–90 21-ps trajectories at each of two or three window positions, took ~1200 CPU h.

Thermodynamic perturbation method

For comparison to the umbrella sampling results, we computed the difference in system energy between formamidinium and guanidinium at representative sites along the translocation pathway and in a 10-Å preequilibrated water ball (Molecular Simulations) by the perturbation dynamics technique (for reviews see McCammon and Harvey, 1987; Straatsma and McCammon, 1992). In each case the system was preequilibrated to 300 K, using 3 ps of heating and 5 ps of equilibration dynamics for each simulation. As with the gramicidin system, no boundary potential was used with the water ball perturbation. Waters remained stable for the duration of the simulations. Hybridization constant values of 0.125, 0.25, 0.5, 0.75, and 0.875 were used to obtain an accurate evaluation of the ensemble average of the perturbation free energy, $F = -RT \ln \langle \exp(^{-}\Delta V/RT) \rangle$; the ensemble was taken from 10-ps production dynamics trajectories. The production dynamics were unconstrained Verlet, except that a window potential (force constant k = 500 kcal/mol·Å^2) was applied to the carbon of the hybrid ion to prevent it from drifting. The hybrid ion contained H in the reactant (formamidinium), NH_2 in the product (guanidinium), and $C(NH_2)_2$ as common atoms for the two ions. This resulted in 10 bonds, 15 bond angles, 18 dihedral angles, and 5 improper dihedral angles in the hybrid ion. All atoms in the peptide dimer and solvent water were also common atoms.

Four representative regions along the translocation path were sampled: the center of the dimer (0 Å), the center of the monomer (6 Å), the entry of the channel (12 Å), and the outside of the channel in the "bulk" water (15 Å). At each position, forward and backward mutations were computed at three different ion starting orientations (0°, 120°, 240° rotations around the channel axis) to improve the sampling of conformational space. It should be pointed out that these orientations do not necessarily correspond to both or even either of those used for the two ions individually in the umbrella sampling study, because here we are using a single hybrid ion. Consequently, we deemed it most appropriate to utilize an average $\Delta\Delta F$ from the forward and backward mutations of all three starting orientations (N = 6).

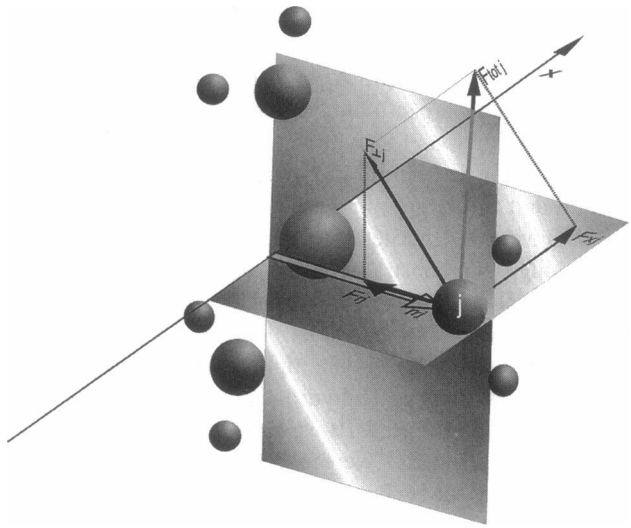

FIGURE 3 Interaction forces acting on individual guanidinium atom j in the gramicidin A channel (channel axis aligned along the x axis). The components of the total force on j, $\mathbf{F}_{tot,j}$, utilized here are the axial force, $\mathbf{F}_{x,j} = \mathbf{F}_{tot,j} \cdot \mathbf{i}$, and the radial force on j, $\mathbf{F}_{r,j}$, given as the component along the radial position vector, $\mathbf{r}_{r,j}$ (perpendicular from the axis to the center of j), of the component of $\mathbf{F}_{tot,j}$ in the plane perpendicular to the axis ($\mathbf{F}_{\perp,j}$): $\mathbf{F}_{r,j} = -(F_{y,j} \cdot r_{y,j} + F_{z,j} \cdot r_{z,j})$.

Force analysis

Force decomposition was performed for the 500-frame ensemble derived from a 10-ps dynamics trajectory by computing the interaction forces between the channel atoms and each of the ion atoms for each frame. The net forces on each of the atoms of the ion were calculated separately (Fig. 3). Then the radial components $F_{r,j}$ (perpendicular to and intersecting with the channel axis) and axial components $F_{x,j}$ (parallel to the channel axis) were summed over the atoms and over the ensemble to yield the net average force on the ion at each window position. Positive radial force was defined as compressive force on the ion, and positive axial force as one pushing the ion out of the channel. The channel axis was defined as the major elliptical axis of the channel backbone.

DelPhi computations

DelPhi (Klapper et al., 1986; Gilson et al., 1988; Gilson and Honig, 1988) is designed to calculate the electrostatic potentials in and around an irregular macromolecular structure (e.g., protein or bilayer) that is embedded in a homogeneous dielectric environment (e.g., water) by solving the Poisson-Boltzmann equation with the finite-difference method. The macromolecular structure is defined as a volume occupied by a set of explicitly defined atoms. The electrostatic energy of the system is given in simplest form (Gilson and Honig, 1988) as

$$E_{elec} = \frac{1}{2} \sum_i q_i \, \phi_i(\epsilon_{in}, \epsilon_{out}) \qquad (5)$$

where ϕ_i (ϵ_{in}, ϵ_{out}) is the potential at the location of q_i estimated from the value at nearby grid points and is a function of the dielectric constants inside and outside of the macromolecule, as well as all of the charges in the system and the ionic strength outside of the macromolecule. DelPhi is actually designed to compute the change in energy due to perturbation of the external dielectric constant, i.e.,

$$\Delta E_{elec} = \frac{1}{2} \sum_i q_i(\phi_i(\epsilon_{in}, \epsilon_{out}) - \phi_i(\epsilon_{in}, \epsilon_{in})) \quad (6)$$

We used DelPhi to compute the neglected long-range interaction energy of the ion with lipid bilayer and bulk electrolyte for correction of the free energy profiles obtained by umbrella sampling. The electrostatic potential energy is an adequate estimate of the potential of mean force correction for this purpose because it is the only significant long-range force.

We verified the appropriateness of DelPhi for the current problem by calculating the potential energy profile for an ion crossing a lipid bilayer. Our results for the latter were essentially identical to those of Neumcke and Läuger (1969), who calculated the same profile by integration of the generalized Nernst-Planck equations.

Because DelPhi was limited to two dielectric regions (defined as internal and external to the regions occupied by atoms of the system), we computed the correction by using two atomic systems (Gilson and Honig, 1988; Bogusz, 1995), as illustrated in Fig. 4. First the volume occupied by the atoms used in the molecular dynamics computations (channel, ion, and explicit waters) was defined as internal (Fig. 4 *a*) and the rest of space as external (probe diameter 3.0 Å), and the energy of modifying the external dielectric from $\epsilon_2 = 2$ to $\epsilon_1 = 1$ (while holding the internal dielectric constant at $\epsilon_2 = 2$) was computed (Fig. 4 *b*):

$$\Delta E_{elec}(\text{no bilayer}, 2, 1) = \frac{1}{2} \sum_i q_i(\phi_i(2, 1) - \phi_i(2, 2)) \quad (7)$$

(Note that the arrow between Figs. 4 *a* and 4 *b* denotes the opposite of the dielectric perturbation energy computed according to Eq. 7.) Then the channel, ion, explicit water

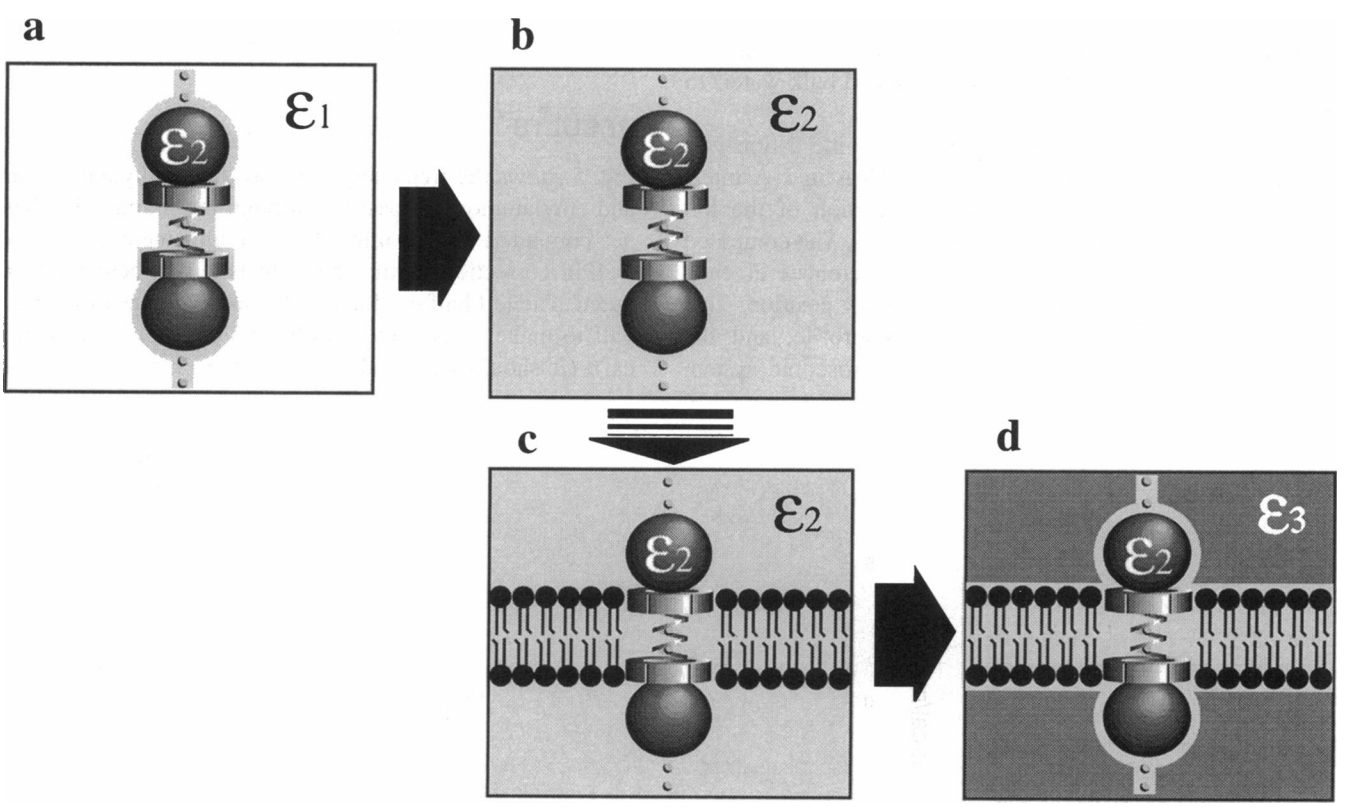

FIGURE 4 Diagram of DelPhi correction structures. First the energy difference between the molecular system used in the molecular dynamics calculations with the vacant surround with a dielectric constant of 1 (representing the conditions for the CHARMM calculations) and the same system with a homogeneous dielectric constant of 2 (the inverse being the energy for going from the system in *a* to that in *b*) is computed. Then the surround is redefined by introducing neutral atoms to occupy the desired bilayer volume, and the energy difference due to a change in the external dielectric constant from 2 to 80 is calculated (from *c* to *d*). The complete perturbation is thus accomplished in two steps. The pair of energy differences can be understood as a pair of perturbations where the perturbation energy is due to the changing interaction of the electric field with the dielectric medium. It thus includes, inherently, the effects of the dielectric structure on the fields, as well as the dielectric's reaction to the fields. Because the two middle structures (*b* and *c*) are electrostatically equivalent (homogeneous dielectric of constant value 2), the inverse of the first perturbation energy summed with the second provides the complete correction for neglected long-range electrostatic terms in the CHARMM calculations. See text concerning the usage of an interior dielectric constant of 2 throughout. Molecular systems are exagerated in size relative to the calculation box.

structure was embedded in a 20-Å-thick set of uncharged atoms representing the bilayer such that internal became bilayer plus channel, ion, and explicit waters (Fig. 4 *c*), and external became the volume occupied only by neglected bulk waters. With this embedded structure the energy of modifying the "external" dielectric constant from $\epsilon_2 = 2$ to $\epsilon_3 = 80$ (while holding the internal dielectric constant at $\epsilon_2 = 2$) was computed (Fig. 4 *d*):

$$\Delta E_{\text{elec}}(\text{with bilayer, 2, 80}) = \frac{1}{2}\sum_i q_i(\phi_i(2, 80) - \phi_i(2, 2)) \quad (8)$$

Because the two reference structures (Fig. 4, *b* and *c*), due to the homogeneous dielectric constant of $\epsilon_2 = 2$, are mathematically equivalent despite the differences in definition of internal and external volumes, the correction energy (i.e., the difference between the energies represented in Fig. 4, *d* and *a*) may be taken as the difference between these two dielectric perturbation energies:

$$\Delta E_{\text{elec}}(1, 80) = \Delta E_{\text{elec}}(\text{no bilayer, 2, 1}) - \Delta E_{\text{elec}}(\text{with bilayer, 2, 80}) \quad (9)$$

This was taken as the neglected energy due to the reaction of the long-range dielectric (both bilayer and bulk water) to the umbrella sampling structure.

This neglected energy was computed as the cation was moved through the channel (from 0 to 16 Å in 1-Å intervals), primarily due to the changing position of the ion relative to the neglected, oriented dielectrics. The computed corrections are thus absolute energy differences at each position and are not relative to any arbitrary position. This correction provides a complete energy profile, and the model can be recategorized as a semimicroscopic system (Dorman et al., 1996). However, it should be noted that the DelPhi grid is finite in volume, so it was necessary to ensure that it was large enough so that the neglected dielectric reaction energy was indeed negligible. The system box, divided into a 65 × 65 × 65 grid, was found to give stable results when the cubic box dimensions were 100 Å on each side, and longer range effects were deemed negligible based on similar results with a 200-Å box.

It should be noted that the molecular dynamics were calculated with $\epsilon = 1$ for the region occupied by the channel, ion, and explicit water rather than $\epsilon = 2$, as was assumed for the start point of our correction (Fig. 4 *a*). However, the neglected energy of interaction between the organic cation and the dielectric medium outside of the simulated system should be reduced somewhat by shielding of the organic cation due to atomic polarizability, which was ignored for the molecular dynamics calculations. The use of $\epsilon = 2$ for the system as the starting point in the DelPhi correction simulates this atomic polarizability shielding.

Complete CHARMM scripts, DelPhi scripts, and "C" programs used to analyze umbrella sampling PMFs are published (Hao, 1996). All computations were done on a Sun Sparc20 Unix workstation with a quad processor or a Silicon Graphics R4000 Indy workstation.

RESULTS

Fig. 5 shows the free energy profiles for methylammonium and ethylammonium passage through the gramicidin channel computed by the umbrella sampling method (without DelPhi correction). Only the right half was actually computed. The left half is added as the mirror image of the right half to make a complete profile (the channel is symmetrical). (It should be noted that the two amine ions are not

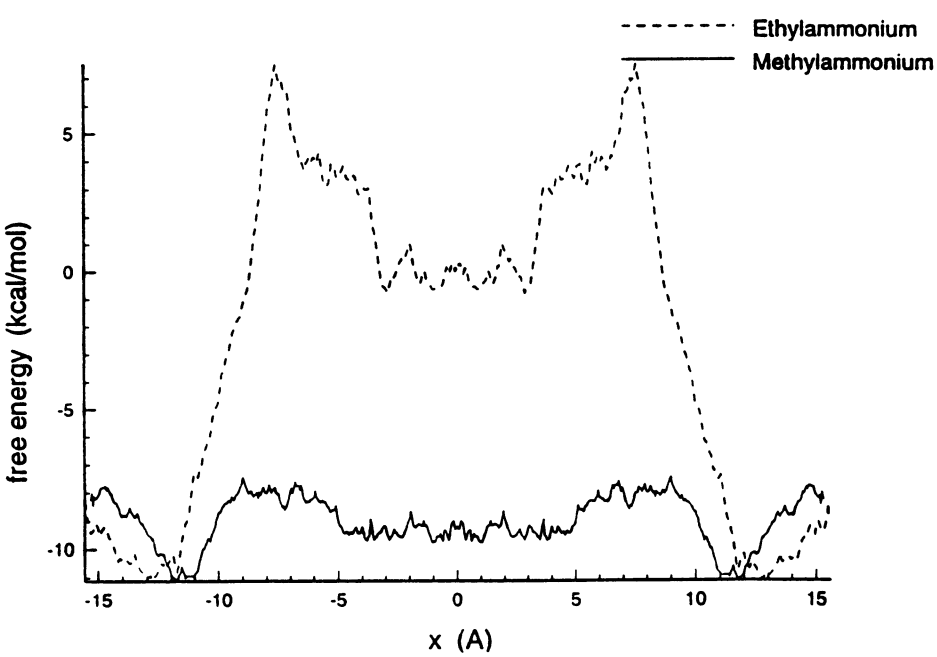

FIGURE 5 Free energy profiles for methylammonium and ethylammonium passage through the gramicidin channel computed by the umbrella sampling method. Only the right half was actually computed. The left half was added as the mirror image to portray the complete profile. For comparison, the methylammonium profile was shifted down, so that its minimum point corresponded to that of ethylammonium.

symmetrical, so that using the mirror image of half the profile is only an approximation. Preliminary computations of complete PMFs for these two ions initially showed dramatic asymmetries in the PMF between the two gramicidin monomer paths, but this was subsequently found to be attributable to cumulative errors in the window-overlap matching procedure and inadequate sampling. With the matching procedure and degree of sampling used here, the asymmetries in the complete PMFs were negligible, except for a slight offset in the position of the steep entry barrier (see below), so for the final computations reported here, only half-windows were computed.) The ζ_1 of $W(\zeta = 0)$ for ethylammonium was arbitrarily set to 0. The methylammonium profile is shifted vertically so that its minimum point corresponds to that of ethylammonium for comparison. There is a broad, 4 kcal/mol free energy activation barrier for methylammonium between the entry (12.5 Å) and the center of the monomer. For ethylammonium, the entry barrier is much larger, ~18 kcal/mol. This is expected from the ionic dimensions and is high enough to prevent this cation from entering the channel on experimental time scales. A decline in the barrier height occurs at the center of the channel, which may reflect the larger flexibility of the channel backbone at the dimer junction (see below). The central energy well is much deeper for ethylammonium than that of methylammonium. This makes sense if the flexibility of the channel is more important for the larger ion.

An energy well of about −3 kcal/mol relative to the most distant position calculated (15 Å) found at the entrance of the channel for both ions may serve as an ion-binding site. The decrease in free energy that occurs as these two ions approach the channel may be partly attributed to the fact that the gramicidin channel actually attracts cations into itself; however, this is primarily due to the neglected long-range electrostatic interactions with bulk water and lipid bilayer, which are not yet included in the simulations (see below).

Fig. 6 compares the free energy profiles for formamidinium and guanidinium in the channel. Again, only the right half was actually computed and the formamidinium profile is shifted vertically to align the two profiles at the channel entry. The entry free energy barrier is found to be 4 kcal/mol for formamidinium and 6.7 kcal/mol for guanidinium. Both barriers are broad, spanning from channel entry to quite near the channel center. An interesting and important feature of the guanidinium profile is that there is a very deep (11.5 kcal/mol below the peak barrier height) free energy well at the center of the dimer. This free energy well, unlike in the cases of methylammonium, ethylammonium, and formamidinium, dwarfs the entry barrier at the channel entry. It is not unique to guanidinium; there is a similar energy well for formamidinium (~3.5 kcal/mol) and guanidinium (~2 kcal/mol).

For all four free energy profiles shown above, fluctuations of 0.2–1 kcal/mol in free energy are found within 1-Å intervals along the entire length of the reaction coordinate. In "flat" regions, no large net force along the channel axis is exerted on the ion because of these fluctuations. Depending on the specific positions of the ion, the net force on the ion can be in either direction. Because of uncertainties about axial rotations of the ion, it is not clear how reproducible these small fluctuations would be; however, the broad features are expected to be quite robust.

With regard to Fig. 5, it should be pointed out that the reaction coordinate is defined as the position of the carbon of methylammonium and the nitrogen of ethylammonium. In each case the amine group is positioned to the right of (i.e., at a greater distance from the channel center than) the carbon. This accounts for the rise in the ethylammonium entry barrier at 12 Å as compared to 11 Å for methylammonium.

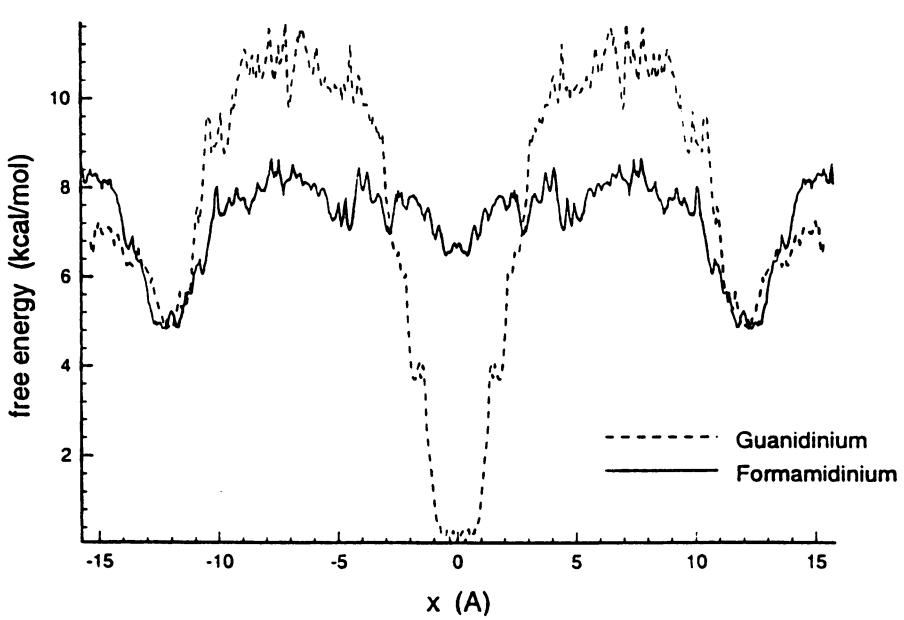

FIGURE 6 Free energy profiles for guanidinium and formamidinium passage through the gramicidin channel, computed by the umbrella sampling method. As in Fig. 5, only the right half was actually computed, and the formamidinium profile was shifted to align the two profiles at the channel entry.

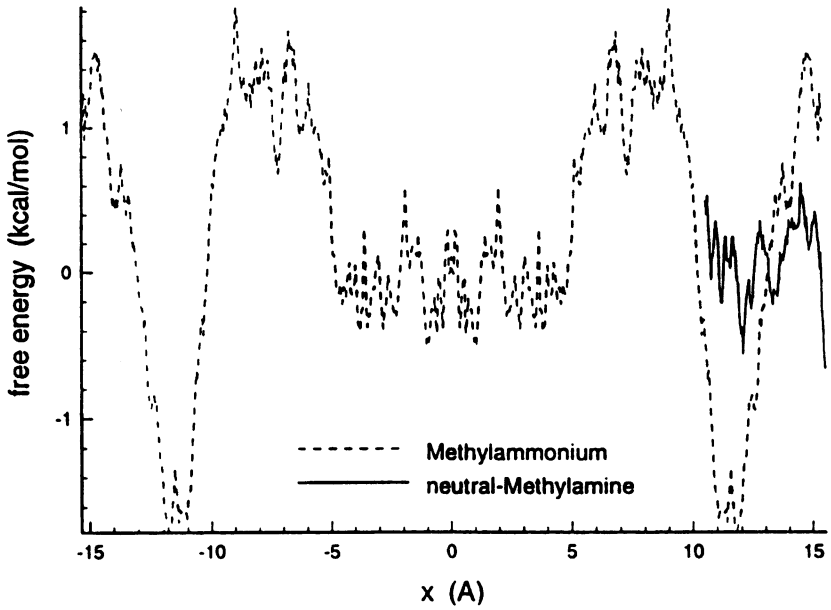

FIGURE 7 A comparison of methylammonium and neutral methylamine profiles at the channel entry. When the positive charge on methylammonium was taken away, the free energy rise external to the channel entry was essentially abolished.

To examine the basis for the energy well outside the channel, a neutral methylamine profile is compared to the charged species (*dashed line*) in Fig. 7. The free energy well is absent for the neutral molecule, indicating that it is electrostatic in origin, but it cannot be determined from this result whether the well is due to attraction to the channel entry or to an artifact of neglecting distant waters.

The corrected free energy profiles shown in Figs. 8 and 9 were constructed by adding a long-range electrostatic correction profile calculated with DelPhi to the corresponding umbrella sampling free energy profiles in Figs. 5 and 6. Fig. 8 shows the profiles for methylammonium and ethylammonium. The activation barrier is increased to ~5.5 kcal/mol for methylammonium and 21 kcal/mol for ethylammonium. For methylammonium, the central well is essentially abolished, whereas the shape of the ethylammonium profile does not change appreciably after correction. The apparent binding site outside the channel is reduced in depth to ~1 kcal/mol for methylammonium and is essentially eliminated for ethylammonium.

In the corrected free energy profiles shown in Fig. 9, the entry barrier increases to 6.2 kcal/mol for formamidinium and to 8.6 kcal/mol for guanidinium. The depth of the central well for formamidinium was nearly eliminated, as in the case of methylammonium. For guanidinium, the well at the channel center is still 11.2 kcal/mol in depth. The

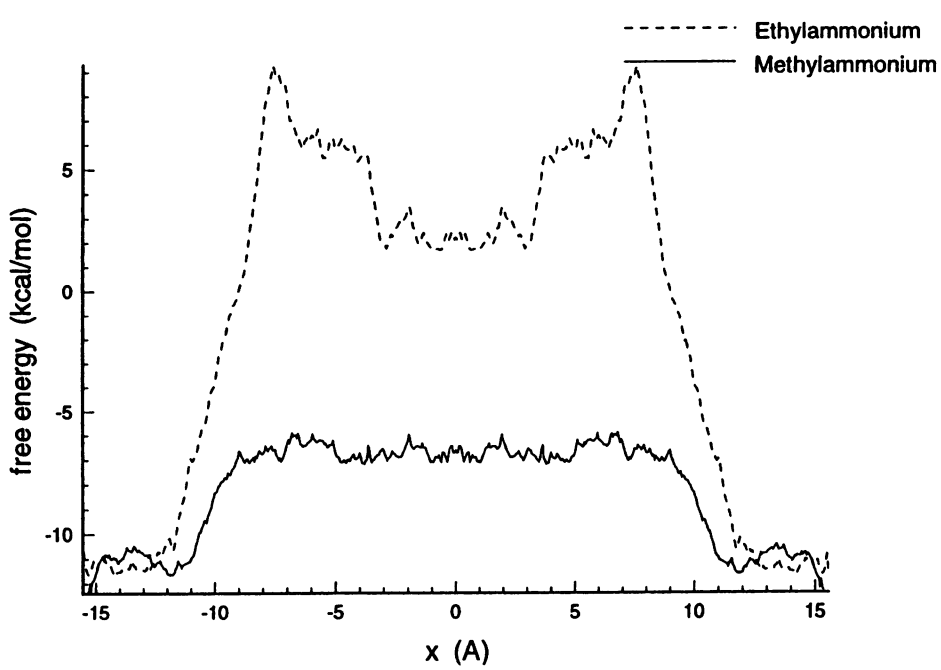

FIGURE 8 Corrected free energy profiles for methylammonium and ethylammonium in the gramicidin channel. DelPhi estimation of the contribution from bulk water and lipid bilayer was added to the corresponding umbrella sampling profiles. The entry barriers are 5.5 kcal/mol for methylammonium and 21 kcal/mol for ethylammonium.

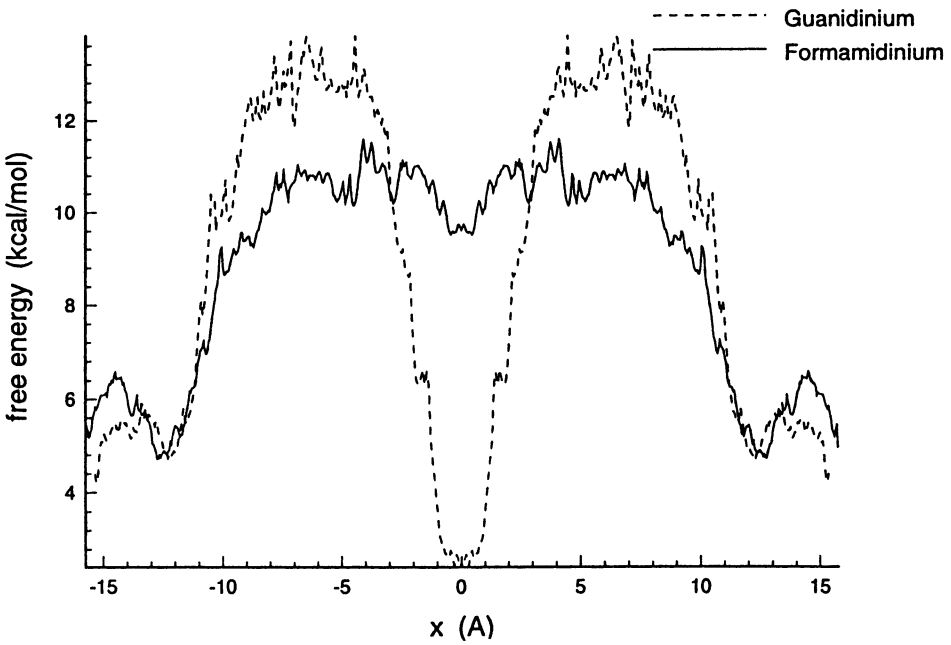

FIGURE 9 Corrected umbrella sampling free energy profiles for formamidinium and guanidinium in the gramicidin channel. A DelPhi estimation of the contribution from bulk water and lipid bilayer was added to the corresponding umbrella sampling profiles. The entry barriers are 6.2 kcal/mol for formamidinium and 8.6 kcal/mol for guanidinium. The formamidinium profile is essentially a single plateau inside the channel like that of methylammonium. In the guanidinium profile there is a deep central well of 11.2 kcal/mol at the channel center.

external wells are also reduced to 1.6 kcal/mol for formamidinium and ~1 kcal/mol for guanidinium.

To evaluate the robustness of the umbrella sampling results, we utilized the conceptually distinct free energy perturbation method. Rather than providing the free energy profile for a single ion, this method yields the free energy difference at a single point along the profile for a pair of ions. Formamidinium and guanidinium were chosen for study because of their close similarity.

The difference in hydration energy (in the absence of a channel) between these two ions was first computed for reference. A water ball of radius 10 Å was used to solvate the hybrid ion (see Model Description). This hybrid ion was originally placed at the center of the water ball without constraint. It did not drift significantly relative to the water ball center during the dynamics simulation. Mutations between formamidinium and guanidinium in both directions were calculated by using the thermodynamic cycle described above, i.e., mutations in vacuum and inside the water ball were calculated separately and $\Delta\Delta F$ was obtained from the difference between these two perturbation energies.

The perturbation results (kcal/mol) are shown in the following cycle:

$$\begin{array}{ccccc} F & + & \text{Solvent} & \Rightarrow & F\cdot\text{Solvent} \\ 17.0 \leftrightarrows - 16.8 & & & & 23.3 \leftrightarrows - 23.6 \\ G & + & \text{Solvent} & \Rightarrow & G\cdot\text{Solvent} \end{array} \quad (10)$$

yielding a difference in the solvation energy of $\Delta\Delta F = 6.6$ kcal/mol. We were unable to identify experimental measures for comparison.

The results of the in-channel perturbation study are shown in Table 1, which reports the six values (three orientations, two mutation directions) of free energy difference at each of four positions along the channel axis. Backward mutations give results similar to the corresponding forward mutations, and ion orientation produces modest variations which, judging by the deviations between forward and reverse mutations, appear to be mainly statistical. The mean was therefore used for comparison to umbrella sampling results.

The $\Delta F_{\text{solvent}}$ for the perturbation in a 10-Å water ball, 23.5 kcal/mol, is below the value obtained with the ion outside the channel in the gramicidin/water system (Table 2,

TABLE 1 ΔF (kcal/mol) versus initial ion axial orientation*

	Formamidinium ⇒ Guanidinium			Guanidinium ⇒ Formamidinium			
x	0°	120°	240°	0°	120°	240°	Mean ± SD
0 Å	27.0	28.0	29.2	−26.6	−27.3	−29.4	27.9 ± 1.2
6 Å	34.3	33.5	36.2	−35.4	−33.1	−32.9	34.2 ± 1.3
12 Å	33.0	30.5	28.8	−30.2	−31.5	−31.3	30.9 ± 1.4
15 Å	27.1	28.7	27.7	−25.7	−26.9	−25.6	27.0 ± 1.2

* The angle is the axial rotation of the ion plane relative to that which bisects the line segment connecting the channel formyl carbons.

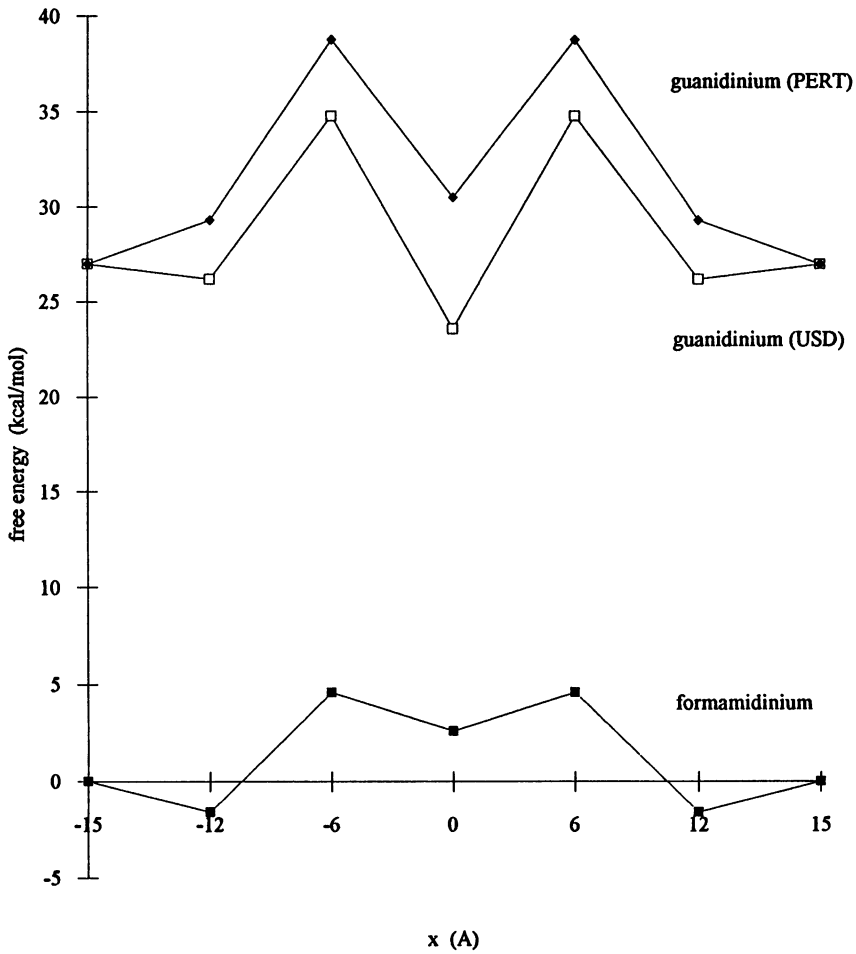

FIGURE 10 Comparison of the free energy results between umbrella sampling and perturbation dynamics. The profiles are simplified to include only representative points, 0, ±6, ±12, and ±15 Å. The bottom curve is the corrected formamidinium profile, which is arbitrarily placed at the x axis. The top curve is the reconstruction of the guanidinium profile according to the perturbation result. The middle curve is the reconstruction of the guanidinium profile at the same level according to the umbrella sampling result.

row 5, for 15 Å), 27.0 kcal/mol. This may be due in part to differences between the water ball outside the channel and the 10-Å water ball used above, or alternatively may suggest influence of the channel on the two ions when they are still 2.5 Å outside of the entrance. Because of this uncertainty, we have chosen to compare the perturbation results to the umbrella sampling results without reference to a pure bulk water state, using x = 15 Å in the gramicidin/water system as a bulk water approximation instead.

Fig. 10 compares the free energy results from umbrella sampling and perturbation dynamics. The umbrella sampling profiles are simplified to include only the representative points 0, ±6, ±12, ±15 Å. The formamidinium umbrella sampling profile (after DelPhi correction; Fig. 9) is arbitrarily placed so that the free energy at ±15 Å is zero. The energy difference between formamidinium and the two guanidinium profiles is 27.0 kcal/mol 15 Å from the free energy perturbation. From the perturbation results shown in Table 1, the guanidinium profile (relative to the formamidinium curve obtained by umbrella sampling) is the top curve in Fig. 10. On the other hand, the guanidinium profile constructed according to the corrected umbrella sampling profile (in Fig. 9), shifted to match the perturbation result at 15 Å, where conditions are nearest to "bulk water," is the middle curve in Fig. 10. Both methods predict a deep well at the center for guanidinium. From the perturbation results one would expect a higher guanidinium free energy profile in general. The height of the activation free energy barrier (from 12 Å to 6 Å) is about the same as expected from umbrella sampling; however, the central well is somewhat shallower.

The discrepancy between the two dynamics methods may be related to two types of errors inherent in the methods. Both are related to the damping of ion orientations in the channel. In both methods the axial rotation of the ion was limited to within 20–40° of the starting position by the short dynamics duration, so the axial rotation was sampled only partially by selecting from three runs with axial rotations differing by 120°. The initial ion orientations in the selected windows differed for the two approaches.

The free energy profile provides only a general picture of the ion permeation through the gramicidin channel. To further explore the ion-channel interaction in these steps, a force decomposition was performed. As described in the Model Description, the radial and axial forces exerted by the system on each atom of the ion were summed over the ion and over the ensemble to yield the net average force on the ion at each window position.

Fig. 11 shows the radial force exerted by the channel on each of the four ions for their trajectories in the right-hand

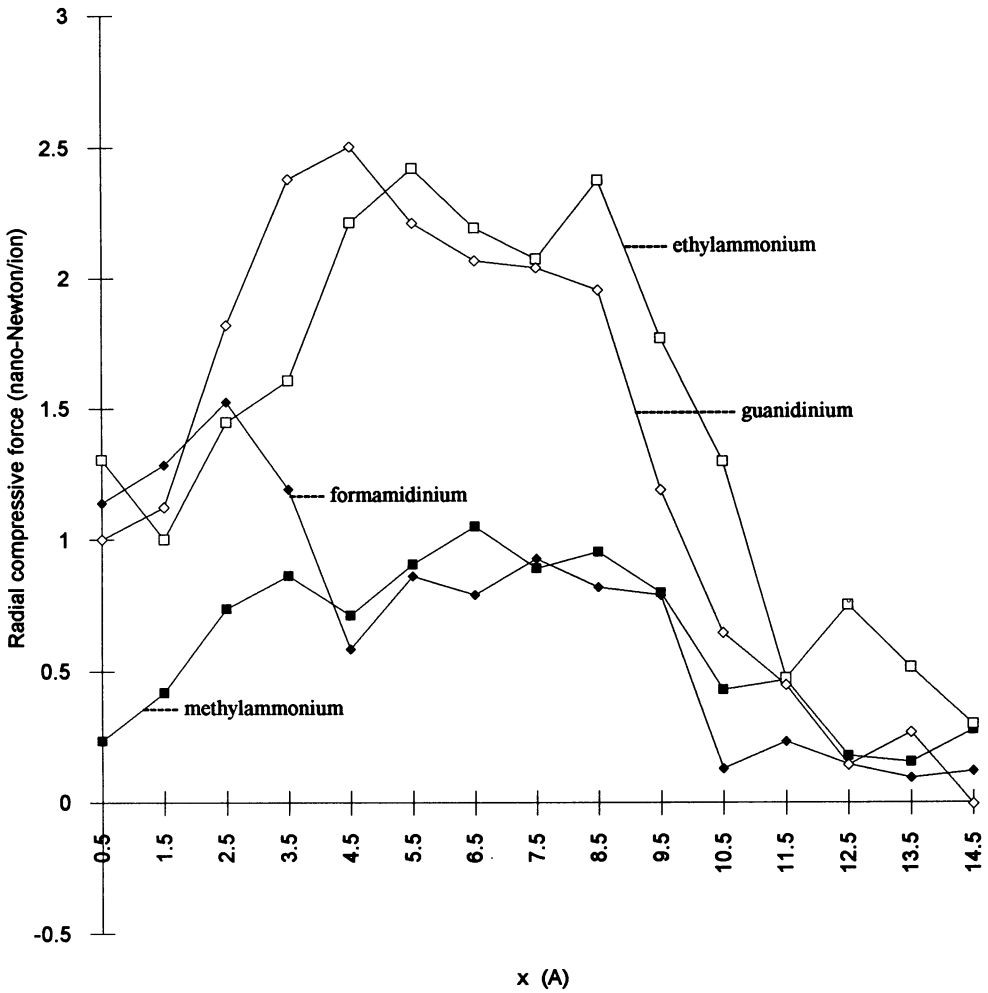

FIGURE 11 Radial components of the forces exerted on the four ions by the channel. Fluctuations are averaged out by taking the mean of the force values for all frames having reaction coordinates within each integer angstrom as the representative force on the midpoint of that angstrom. The standard deviation is usually 2–4 times smaller than the magnitude of each value. Only the right half is calculated and shown.

monomer. To average out the fluctuations, values within each integral angstrom were averaged and the mean was taken as the representative force at the midpoint of each angstrom. The standard deviation was 2–4 times less than the typical magnitude. A positive value corresponds to a compressive radial force on the ion by the channel. The channel exerts a compressive force on each of the four ions when they are within the channel (0 Å to 10.5 Å). Channel compression drops toward zero as the ion leaves the channel (11.5 Å to 14.5 Å) and is diminished at the dimer junction, especially for ethylammonium and guanidinium. The force was level and high (2–2.5 nN/ion) between 3.5 and 9.5 Å for the larger ions, guanidinium and ethylammonium, consistent with the high entry barriers and high free energy levels inside the channel for these two ions (Figs. 5, 6, 8, 9). The lower compressive forces on methylammonium and formamidinium are in accord with the observation that these ions readily permeate, in agreement with the lower activation barriers and energy levels inside the channel. The drop at the center of the channel in the radial compressive forces on the two larger ions directly implies increased flexibility at the dimer junction. The formamidinium curve shows an unexpected increase in the magnitude of the compressive force at the dimer junction of unknown origin. We therefore propose that the radial compression of the ion by the channel is a useful quantitative measure of steric hindrance. As Fig. 11 illustrates, steric hindrance is an important component of the selectivity between the two larger ions and the two smaller ones.

Fig. 12 shows the axial components of the forces exerted by the channel on the ions. This is expected to be related (but not identical) to the first derivative of the free energy profile. The same kind of ensemble average as used in Fig. 11 was performed, except in this case the standard deviation is much larger than in the previous one, about equal to the average magnitude. A positive value denotes that the channel pushes the ion to the right, i.e., out of the channel, whereas a negative value denotes that the channel pulls the ion in toward the center of the channel. It can be seen that, except for formamidinium, the channel exerts an attractive

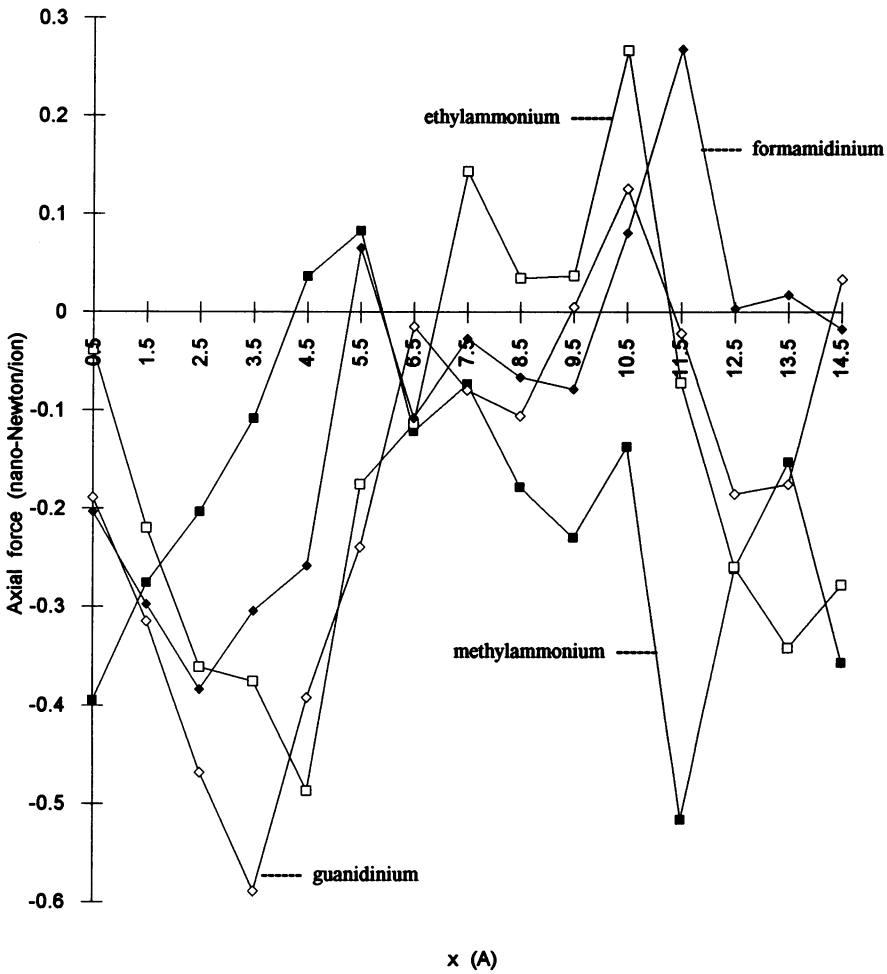

FIGURE 12 Axial components of the forces exerted on the four ions by the channel. Fluctuations are averaged out by taking the mean of the force values within each integer angstrom as the representative force on the midpoint of that angstrom. The standard deviation is usually of the same magnitude as the values themselves. Only the right half is calculated and shown.

force on the cations when they are external (12.5 Å to 14.5 Å). At the channel entry (10.5–11.5 Å), there is an extruding force on formamidinium, ethylammonium, and guanidinium, but an attractiion for methylammonium. This is consistent with the fact that methylammonium has a cylindrical shape with length 4 Å and diameter 3.1 Å. The other three ions have minimal dimensions greater than the inner diameter of the regular $\beta^{6.3}$ helix and are expected to force the channel open as they enter. Thus the positive axial force at the channel entry is another indication of steric hindrance. At the center of the channel, forces on all four ions are negative, i.e., they point to the dimer junction. This further indicates that the dimer junction is a region of channel wall flexibility. The attracting force on guanidinium exhibits the largest magnitude at 2.5 Å and 3.5 Å because of the increasing potential for hydrogen bond formation as the ion nears the dimer junction, and accounts for the deep central energy well in the guanidinium profile (Figs. 6 and 9).

DISCUSSION

The molecular dynamics calculations are successful in that

1. The passage barriers for methylammonium and formamidinium are low, consistent with permeability, whereas that of the impermeant cation, ethylammonium, is high, and that of the quasipermeable guanidinium is intermediate.

2. An expected strong guanidinium-binding site in the center of the channel is observed and explained in terms of steric and hydrogen-bonding factors.

3. The steric hindrance to ion passage is evaluated quantitatively in terms of the radial compressive force on the ion.

These qualitative results are very gratifying, and are solidly attested in the results, despite the difficulties associated with non-spherical ligands. For instance, umbrella sampling and perturbation dynamics both yielded a unique deep central well for guanidinium, and this well is approximately the depth expected from the increased hydrogen bonding observed for guanidinium at the dimer junction.

From a quantitative viewpoint, there are some weaknesses in the interpretation of the experimental data and discrepancies between the computed free energy profiles and those deduced from experiment. These can be summarized as

1. The deduction that a binding site for guanidinium exists at the center of the channel (based on indications from voltage dependence in channel blocks and the channel symmetry) deserves closer experimental examination.

2. The height of the barrier for exiting the putative central binding site is based on an arbitrary assumption about the transmission coefficient in Eyring rate theory (Hemsley and Busath, 1991).

3. The computed entry barrier for guanidinium appears to be too low, relative to that for formamidinium, by ~4 kcal/mol. These issues will be discussed next in more detail, starting with a more detailed description of the commonality between guanidinium transport experiment and theory.

The free energy profile for guanidinium is more complicated than for methylammonium or formamidinium (Fig. 9). There is a high activation energy barrier of 8.6 kcal/mol that limits the guanidinium entry, and a deep energy well of 11.2 kcal/mol that prevents exit once it gets in. In experiments, Hemsley and Busath (1991) found that guanidinium causes flicker blocks of potassium currents in the normal gramicidin channel. The average block duration is shortened as membrane potential is increased. This relief of block indicates that the blocking ion passes through the channel rather than lodging in the entry. The voltage dependence of the block rate suggests that the barrier to the blocking site is effectively 40–48% into the membrane field. The voltage dependence of the block duration suggests a barrier to blocker exit 24% down the membrane field from the blocking site. The entry barrier was estimated by comparison between guanidinium block rate and formamidinium passage rate to be 8.6 kcal/mol higher for guanidinium than for formamidinium. The exit barrier for guanidinium, based on Eyring rate theory analysis of the block durations (using the arbitrary value of 0.1 for the transmission coefficient), was estimated to be 13.1 kcal/mol. These results, synthesized into a free energy barrier pattern (reproduced as Fig. 13), present a pattern that is similar in appearance to the one presented in Fig. 9. In both profiles there is a large entry barrier and a deep well at the center of the channel. Even the amplitudes and positions of the barrier and well appear to be similar.

However, it should be pointed out that some of these similarities are fortuitous or even misleading. The entry barrier height predicted from experiment in Fig. 13 is relative to the formamidinium entry barrier and therefore should be compared to the difference between guanidinium and formamidinium barriers from Fig. 9, which averages to

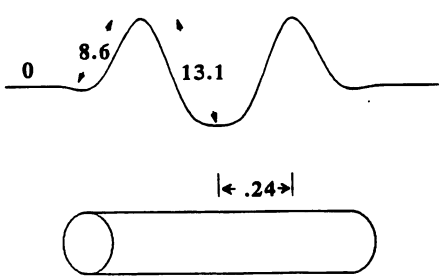

FIGURE 13 Experimentally deduced free energy profile for guanidinium (relative to formamidinium) based on potassium current block data. Reproduced with permission from Hemsley and Busath (1991).

~2.2 kcal/mol rather than the 8.6 kcal/mol in Fig. 13. On the other hand, this predicted entry barrier is quite similar to one obtained with perturbation dynamics. The perturbation energy at 6.0 Å (relative to 15.0 Å) is 7.2 kcal/mol (Table 1).

The position of the entry barrier in Fig. 13 is a compromise between two conflicting experimental facts: the voltage dependence and low value of the guanidinium entry rate suggest a large peak 48% of the way into the channel (i.e., near the dimer junction), but the voltage dependence and low value of the exit rate suggest that the ion must travel 24% of the way through the channel to get from the strong binding site to the peak of the exit barrier. Channel symmetry demands that the exit barrier be a mirror image of the entry barrier, so it is logical to conclude that there must be a large well at 50%, with entry and exit barriers located at about 25% and 75%. The discrepancy, especially with the positioning of the entry barrier, could be due to experimental inaccuracy (e.g., time resolution) or inadequacy of theory (e.g., failure to account for blocks produced by incomplete entry barrier crossings). The latter would produce an enhanced voltage dependence of block and would require predictions from Brownian dynamics rather than the Eyring rate theory that was used.

Finally, the height of the exit barrier, relative to the formamidinium "exit barrier" (~1 kcal/mol), is seen in Fig. 9 to be ~12 kcal/mol, which is very close to the value of 11.6 kcal/mol predicted by experiment. However, this should be viewed as a largely fortuitous agreement. The experimental estimate was based on Eyring rate theory, with an arbitrarily assigned transmission coefficient value of 0.1. This value, computed with activated dynamics for the short movement of Na^+ within the channel, was considered an upper limit for guanidinium passage over the broad barrier. A transmission coefficient an order or two of magnitude lower would have been as plausible, which would have suggested a 4–8 kcal/mol lower exit barrier. Concerning the same issue, the perturbation dynamics results reported here in Fig. 10 yielded a somewhat lower exit barrier for guanidinium (relative to formamidinium), ~9 kcal/mol.

In light of the present results, these issues must be reexamined. In particular, improved time resolution of the experiments is crucial and blocking behaviors must be more tightly related to barrier properties by using Brownian dynamics and activated molecular dynamics. Furthermore, studies of the temperature dependence of block should be very revealing, given the tight constraints the channel imposes on guanidinium in the narrowest region, where the very regular channel hydrogen-bonding pattern should restrain channel conformational variability, in contrast to the relative freedom of both ion and channel expected at the dimer junction. Nevertheless, both methods suggest that guanidinium resides at the dimer junction during blocking episodes.

To evaluate the atomic mechanism of guanidinium binding at the dimer junction, we computed the radial density histogram for distances between ionic charged hydrogens and channel or water oxygens by using the ensemble of

configurations generated by the umbrella sampling dynamics trajectories for each of the four ions. From these histograms, the average number (per ion) of separations between 0 and 2.5 Å (i.e., the ensemble average number of hydrogen bonds formed between the ion and all neighboring oxygens) was extracted and is shown in Table 2 for each of two representative positions on the reaction pathway, the center of the channel (0 Å) and the center of one monomer (6 Å). In the center of the monomer the number of hydrogen bonds correlates with the number of cation hydrogen bond donors, i.e., 3, 3, 4, and 6 for the four ions, respectively. However, at the dimer junction (0 Å) there is a reduction by ~1 in the number of hydrogen bonds formed by the first three ions and an increase by 1.5 in the number formed by guanidinium. At the center of a monomer (6 Å), all four ions are in close contact with the channel wall on all sides. Judging from the free energy profiles, radial forces, and axial forces for the larger two cations, guanidinium and ethylammonium, the channel center (0 Å) is more spacious, consistent with the measurements of Smart et al. (1993). Methylammonium, ethylammonium, and formamidinium have fairly compact polar hydrogens that tend to hug one wall in this region and actually decrease their hydrogen bonding to the carbonyls. On the other hand, the three polar NH_2 groups in guanidinium project away from the central carbon in a trigonal planar conformation such that the ion cannot hug one wall, but continues, even at the center of the channel, to contact the channel walls on all sides. The extra space at the dimer junction apparently provides guanidinium greater than usual hydrogen bonding potential, explaining the increased number of observed hydrogen bonds in Table 2. Guanidinium acts like an octopus at the dimer junction, using all six donors and taking advantage of the junctional flexibility to extensively engage the channel acceptors. The increase by 1.5 hydrogen bonds over the number at $x = 6$ Å could reasonably be expected to yield up to 7.5 kcal/mol of well depth. The remainder of the dimer junction well depth could be due to reduced compression by the channel. An alternative comparison is to compare the 7.3 hydrogen bonds formed by guanidinium at the dimer junction to the 4.3 formed by formamidinium: the difference of 3 easily explains the guanidinium central well depth relative to formamidinium.

Weak ion-binding sites for all four cations are found outside the channel (~12 Å from the channel center). Before long-range electrostatic corrections, apparent binding affinity is very high for all four ions (3–3.5 kcal/mol, Figs. 5 and 6). This is consistent with the deep binding sites computed for Na^+ in the same region (Roux and Karplus, 1993; Åqvist and Warshel, 1989), which reflected an attractive field for cations from the ethanolamine and carbonyl oxygens positioned at the channel entry. A neutral methylamine was therefore constructed to test this assumption. As shown in Fig. 7, the binding site disappears when the charge on methylammonium is removed. This confirms that the apparent binding affinity for organic cations is indeed electrostatic in nature. However, further analysis of neglected long-range factors demonstrates that the neglected long-range solvent and lipid bilayer, which are also electrostatic in origin, contribute most to the apparent external binding affinity. We cannot assess how much of the apparent sites for Na^+ in the prior studies mentioned above might be an artifact of neglect of distant waters. Both of the above-mentioned studies used slabs of thickness comparable to our explicit water balls.

TABLE 2 Average hydrogen bond count ($R_{H\text{-}O} \leq 2.5$ Å)

	$x = 0$ Å	$x = 6$ Å
Methylammonium	3.4	4.3
Ethylammonium	4.5	5.4
Formamidinium	4.3	5.6
Guanidinium	7.3	5.8

The free energy perturbation calculations yield a PMF difference similar to that seen with umbrella sampling. The latter could suffer from cumulative errors because we always picked the shallowest profile from the different starting ion orientations to include in the pieced-together free energy profile. This may especially affect the height of the entry barrier to guanidinium, where each section was generally quite steep. For instance, before implementing this selection procedure (based on a single rotational orientation), we had estimated the entry barrier for guanidinium to be higher than that of formamidinium by 2.6 kcal/mol (Pear and Busath, 1990) and 6 kcal/mol (Hao and Busath, 1995) in two preliminary computations, with the total height of the entry barrier to guanidinium being >18 kcal/mol in the latter computation. The selection criteria used here were based on the rationale that the ion would follow the course of least resistance, rotating to adapt to the channel at each position. This introduces an uncertainty that we cannot assess.

The perturbation dynamics model is not susceptible to cumulative errors; however, the positions of equivalent atoms in the two compounds were constrained by the method to be at the same sites, whereas the atoms that differed between the compounds moved independently of each other. This has the effect of requiring the formamidinium ion to assume the same axial rotation in the channel as the guanidinium, which may be an overly restrictive assumption. Furthermore, preliminary tests suggest that more extensive dynamics runs may yield somewhat greater free energy differences, indicating that the perturbation results reported here may not reflect a completely equilibrated system; rather they should be viewed as an initial estimate.

We have not directly analyzed the differences in dehydration energy for the four ions (i.e., the ion-water interaction energy, corrected for long-range interactions, outside versus inside the channel). Hence it can reasonably be supposed that these would decrease in the sequence guanidinium > formamidinium > methylammonium > ethylammonium, based on examination of the structures with respect to polarity and hydrogen bond donors. Guanidinium has the most donors; ethylammonium is the most hydropho-

bic, with both a methylene and a methyl group. That dehydration forces make an important contribution is evident, however, when the axial force plot is compared to the free energy profile. According to the free energy profiles, methylammonium is under a net outward force (negative free energy gradient) in the region of the entry (9–12 Å). The total free energy profile must include an outward potential of mean force from the waters that exceeds the inward force exerted by the channel to yield an entry barrier for methylammonium. Therefore we conclude that the entry barrier for methylammonium is mainly due to dehydration, whereas size exclusion plays a more significant role for formamidinium, guanidinium, and ethylammonium entry.

In addition to confirming the main features of guanidinium and formamidinium transport reported preliminarily (Pear and Busath, 1990), we have evaluated the profiles for methylammonium and ethylammonium, computed perturbation energies to cross-check the umbrella sampling results, corrected for long-range electrostatic contributions of neglected solvent, analyzed radial and axial forces of the channel on the ions, and examined hydrogen bond formation between channel and ions. Our results show that the long-range bulk water is very important. The force and hydrogen bond analyses indicate a steric barrier to entry of all but methylammonium, compression of all of the ions within the channel by the channel walls, increased flexibility at the dimer junction, and an increase in hydrogen bond formation for guanidinium (but not the other three ions) at the dimer junction. It is interesting to note that the current experimentally derived structures for the gramicidin channel differ considerably in pore diameter and that guanidinium block behavior, in conjunction with computations such as these, may provide an alternative method of distinguishing between such models and/or assessing the dynamic backbone flexibility in the gramicidin channel.

We thank Andrea Dorigo and Jim Fukuda for preliminary analyses, James Ricks for graphics rendering and text editing, Donald Marsh for use of his Sun workstation, and Peter Jordan for helpful discussions. CHARMM was licensed from Martin Karplus at Harvard University, and DelPhi from Anthony Nicholls, Barry Honig and colleagues, Columbia Univesity. Molecular Simulations WebLab Viewer was used to create Fig. 2, and Quanta was used during the project for molecular graphics and analysis.

REFERENCES

Åqvist, J., and A. Warshel. 1989. Energetics of ion permeation through membrane channels. Solvation of Na^+ by gramicidin A. *Biophys. J.* 56:171–182.

Arseniev, A. S., A. L. Lomize, I. L. Barsukov, and V. F. Bystrov. 1986. Gramicidin A transmembrane ion-channel. Three-dimensional structure reconstruction based on NMR spectroscopy and energy refinement. *Biol. Membr.* 3:1077–1104.

Bamberg, E., and P. Läuger. 1974. Temperature-dependent properties of gramicidin A channels. *Biochim. Biophys. Acta.* 367:127-133.

Becker, M. D., R. E. Koeppe, II, and O. S. Andersen. 1992. Amino acid substitution and ion channel function. Model-dependent conclusions. *Biophys. J.* 62:25-27.

Bogusz, S. J. 1995. Molecular computations on structure and selectivity of β-barrel models for the voltage-gated potassium, sodium, and calcium channels' pore regions. Ph.D. thesis. Brown University, Providence, RI.

Brooks, B. R., R. E. Bruccoleri, B. D. Olafson, D. J. States, S. Swaminathan, and M. Karplus. 1983. CHARMM: a program for macromolecular energy, minimization, and dynamics calculations. *J. Comput. Chem.* 4:187-217.

Busath, D. D. 1993. The use of physical methods in determining gramicidin channel structure and function. *Annu. Rev. Physiol.* 55:473–501.

Busath, D., G. Hemsley, T. Bridal, M. Pear, K. Gaffney, and M. Karplus. 1988. Guanidinium as a probe of the gramicidin channel interior. *In* Transport through Membranes: Carriers, Channels and Pumps. A. Pullman, J. Jortner, and B. Pullman, editors. Kluwer Academic Publishers, Dordrecht, Boston, and London. 187-201.

Crouzy, S., T. B. Woolf, and B. Roux. 1994. A molecular dynamics study of gating in dioxolane-linked gramicidin A channels. *Biophys. J.* 67: 1370-1386.

Dorman, V., M. B. Partenskii, and P. C. Jordan. 1996. A semi-microscopic Monte Carlo study of permeation energetics in a gramicidin-like channel: the origin of cation selectivity. *Biophys. J.* 70:121–134.

Durkin, J. T., L. L. Providence, R. E. Koeppe II, and O. S. Andersen. 1992. Formation of non-$\beta^{6.3}$-helical gramicidin channels between sequence-substituted gramicidin analogs. *Biophys. J.* 62:145–159.

Eisenman, G., and R. Horn. 1983. Ionic selectivity revisited: the role of kinetic and equilibrium processes in ion permeation through channels. *J. Mol. Biol.* 767:197–225.

Eisenman, G., S. Krasne, and S. Ciani. 1976. Further studies on ion selectivity. *In* Ion and Enzyme Electrodes in Medicine and in Biology. M. Kessler, L. Clark, D. Lubbers, I. Silver, and W. Simon, editors. Urban and Schwarzenberg, Munich, Berlin, and Vienna. 3–22.

Eisenman, G., and J. P. Sandblom. 1983. Energy barriers in ionic channels: data for gramicidin A interpreted using a single-file (3B4S″) model having 3 barriers separating 4 sites. *In* Physical Chemistry of Transmembrane Ion Motions. G. Spach, editor. Elsevier North-Holland Biomedical Press, Amsterdam. 329-347.

Etchebest, C., and A. Pullman. 1988. Energy profile of Cs^+ in gramicidin A in the presence of water. Problem of the ion selectivity of the channel. *J. Biomol. Struct. Dyn.* 5:1111–1125.

Etchebest, C., S. Ranganathan, and A. Pullman. 1984. The gramicidin A channel: comparison of the energy profiles of Na^+, K^+ and Cs^+. Influence of the flexibility of the ethanolamine end chain on the profiles. *FEBS Lett.* 173:301–306.

Eyring, H., R. Lumry, and J. W. Woodbury. 1949. Some applications of modern rate theory to physiological systems. *Record Chem. Prog.* 10: 100–114.

Gilson, M., and B. Honig. 1988. Calculation of the total electrostatic energy of a macromolecular system: solvation energies, binding energies, and conformational analysis. *Proteins Struct. Funct. Genet.* 4:7-18.

Gilson, M., K. Sharp, and B. Honig. 1988. Calculating electrostatic interactions in bio-molecules: method and error assessment. *J. Comput. Chem.* 9:327-335.

Hao, Y. 1996. Molecular dynamics study of free energy profiles for permeation of small organic cations in gramicidin A channel. Ph.D. Thesis. Brown University, Providence, RI.

Hao, Y., and D. Busath. 1995. Free energy profile for small organic cations in gramicidin A channel with umbrella sampling and perturbation dynamics. *Biophys. J.* 68:A151.

Hao, Y., and D. D. Busath. 1996. Free energy profiles for organic cations in gramicidin A channels. *Biophys. J.* 70:A80.

Hemsley, G., and D. Busath. 1991. Small iminium ions block gramicidin channels in lipid bilayers. *Biophys. J.* 59:901-907.

Hille, B. 1992. Ionic Channels of Excitable Membranes, 2nd ed. Sinauer Associates, Sunderland, MA.

Jordan, P. C. 1987. Microscopic approaches to ion transport through transmembrane channels. The model system gramicidin. *J. Phys. Chem.* 91:6582–6591.

Jordan, P. C. 1990. Ion-water and ion-polypeptide correlations in a gramicidin-like channel. A molecular dynamics study. *Biophys. J.* 58:1133-1156.

Jorgensen, W. L., J. Chandrasekhar., J. D. Madura, R. W. Impey, and M. L. Klein. 1983. Comparison of simple potential functions of simulating lipid water. *J. Chem. Phys.* 79:926-935.

Ketchum, R. R., K.-C. Lee, S. Huo, and T. A. Cross. 1996. Macromolecualar structural elucidation with solid state NMR derived orientational constraints. *J. Biomol. NMR.* 8:1–14.

Kim, K. S., D. P. Vercauteren, M. Welti, S. Chin, and E. Clementi. 1985. Interaction of K^+ ion with the solvated gramicidin A transmembrane channel. *Biophys. J.* 47:327-335.

Klapper, I., R. Hagstrom, R. Fine, K. Sharp, and B. Honig. 1986. Focusing of electric fields in the active site of Cu-Zn superoxide dismutase: effects of ionic strength and amino-acid modification. *Proteins Struct. Funct. Genet.* 1:47-59.

Koeppe, R. E., II, L. L. Providence, D. V. Greathouse, F. Heitz, Y. Trudelle, N. Purdie, and O. S. Andersen. 1992. On the helix sense of gramicidin A single channels. *Proteins.* 12:49–62.

Läuger, P. 1973. Ion transport through pores. A rate-theory analysis. *Biochim. Biophys. Acta.* 311:423–441.

Levitt, D. G. 1982. Comparison of Nernst-Planck and reaction-rate models for multiply occupied channels. *Biophys. J.* 37:575–587.

Levitt, D. G. 1991. General continuum theory for multiion channel. I. Theory. *Biophys. J.* 59:271–277.

McCammon, J. A., and S. C. Harvey. 1987. Dynamics of Proteins and Nucleic Acids. Cambridge University Press, Cambridge.

Momany, F. A., and R. Rone. 1992. Validation of the general purpose Quanta 3.2/CHARMm Force Field. *J. Comp. Chem.* 13:888–900.

Myers, V. B., and D. A. Haydon. 1972. Ion transfer across lipid membranes in the presence of gramicidin A. II. The ion selectivity. *Biochim. Biophys. Acta.* 274:313–322.

Neumcke, B., and P. Läuger. 1969. Nonlinear electrical effects in lipid bilayer membranes. II. Integration of the generalized Nernst-Planck equations. *Biophys. J.* 9:1160–1170.

Northrup, S. H., M. R. Pear, C.-Y. Lee, J. A. McCammon, and M. Karplus. 1982. Dynamical theory of activated processes in globular proteins. *Proc. Natl. Acad. Sci. USA.* 79:4035-4039.

Patey, G. N., and J. P. Valeau. 1975. A Monte Carlo method for obtaining the interionic potential of mean force in ionic solution. *J. Chem. Phys.* 63:2334–2339.

Pear, M., and D. Busath. 1990. Free energy profile for iminium transport by gramicidin: guanidinium vs. formamidinium. Abstract. *In* Proceedings of the 10th International Biophysics Congress. P5.5.7.

Roux, B. 1990. Theoretical study of ion transport in the gramicidin A channel. Ph.D. thesis. Harvard University, Cambridge, MA.

Roux, B., and M. Karplus. 1991a. Ion transport in a gramicidin-like channel: structure and thermodynamics. *Biophys. J.* 59:961-981.

Roux, B., and M. Karplus. 1991b. Ion transport in a gramicidin-like channel: dynamics and mobility. *J. Phys. Chem.* 95:4856-4868.

Roux, B., and M. Karplus. 1993. Ion transport in the gramicidin channel: free energy of the solvated right-handed dimer in a model membrane. *J. Am. Chem. Soc.* 115:3250-3260.

Roux, B., and M. Karplus. 1994. Molecular dynamics simulations of the gramicidin channel. *Annu. Rev. Biophys. Biomol. Struct.* 23:731–761.

Saberwal, G., O. S. Andersen, D. V. Greathouse, and R. E. Koeppe, II. 1995. Sequence determinants of gramicidin channel folding. *Biophys. J.* 68:A151.

Seoh, S-A., and D. Busath. 1993a. The permeation properties of small organic cations in gramicidin A channels. *Biophys. J.* 64:1017-1028.

Seoh, S-A., and D. Busath. 1993b. Formamidinium-induced dimer stabilization and flicker block behavior in homo- and heterodimer channels formed by gramicidin A and *N*-acetyl gramicidin A. *Biophys. J.* 65: 1817-1827.

Seoh, S-A., and D. D. Busath. 1995. Gramicidin tryptophans mediate formamidinium-induced channel stabilization. *Biophys. J.* 68: 2271–2279.

Smart, O. S., J. M. Goodfellow, and B. A. Wallace. 1993. The pore dimensions of gramicidin A. *Biophys. J.* 65:2455–2460.

Straatsma, T. P., and J. A. McCammon. 1992. Computational alchemy. *Annu. Rev. Phys. Chem.* 43:407-435.

Tucker, W. A., T. G. Fletcher, J. F. Hinton, and G. Harms. 1992. Three dimensional structure of gramicidin in SDS micelles. *Biophys. J.* 61: A525.

Turano, B., M. Pear, and D. Busath. 1992. Gramicidin channel selectivity: molecular mechanics calculations for formamidinium, guanidinium, and acetamidinium. *Biophys. J.* 63:152-161.

Urban, B. W., and S. B. Hladky. 1979. Ion transport in the simplest single-file pore. *Biochim. Biophys. Acta.* 554:410-429.

Urry, D. W. 1984. On the molecular structure of the gramicidin transmembrane channel. *In* The Enzymes of Biological Membranes, 2nd ed, Vol. 1. A. N. Martanosi, editor. Plenum, New York. 229–257.